

## Comparative planetary mineralogy: Pyroxene major- and minor-element chemistry and partitioning of vanadium between pyroxene and melt in planetary basalts

JIM KARNER,\* J.J. PAPIKE, AND C.K. SHEARER

Institute of Meteoritics, Department of Earth and Planetary Sciences, University of New Mexico, Albuquerque, New Mexico 87131-1126, U.S.A.

### ABSTRACT

Pyroxene grains from 14 basalt suites from the Earth, Moon, Mars, and Vesta were studied by electron- and ion-microprobe techniques. The results show that several elemental trends can be related to planetary parentage and crystallization conditions including paragenetic sequence and kinetics. Ferric iron ( $\text{Fe}^{3+}$ ) systematics show that terrestrial pyroxene is enriched in  $\text{Fe}^{3+}$  compared with pyroxene from Mars due to higher oxygen fugacity ( $f_{\text{O}_2}$ ) conditions on the Earth that produce more  $\text{Fe}^{3+}$  in basaltic melts. Low  $f_{\text{O}_2}$  conditions on the Moon and Vesta result in very little or no  $\text{Fe}^{3+}$  in pyroxene from these bodies. Terrestrial pyroxenes contain more Na than those from Mars, yet martian plagioclase contains more Na than terrestrial. This difference is because terrestrial pyroxene contains more  $\text{Fe}^{3+}$  and thus the acmite component ( $\text{NaFe}^{3+}\text{Si}_2\text{O}_6$ ) is more important on Earth than Mars. Pyroxenes from the Moon and Vesta have very little Na, which can be attributed to the overall volatile-depleted nature of these bodies. All planetary pyroxenes show that Cr decreases with increasing fractionation because it is compatible in pyroxene, and in many basalts the crystallization of chromite depletes the melt in  $\text{Cr}^{3+}$ . The  $\text{Mn}/\text{Fe}^{2+}$  systematics in pyroxene show distinct trends for the planetary bodies in the order Vesta > Mars > Earth > Moon. These  $\text{Mn}/\text{Fe}^{2+}$  trends are most likely affected by the volatility of Mn relative to Fe, and thus there is an increase in the Mn/Fe ratio with increasing distance from the Sun, except for the Moon, which likely lost Mn during its giant impact origin. These same trends have been documented for olivine from the different planets, and this parameter as measured in basaltic silicates is a robust fingerprint of planetary parentage. Vanadium partitioning into planetary pyroxene grains is affected by oxygen fugacity, the availability of charge-balancing elements, basaltic crystallization sequences, and kinetics. Partitioning of V into pyroxene at low  $f_{\text{O}_2}$  conditions (i.e., Moon and Vesta) is seen to increase as the charge-balancing cation  $^{\text{IV}}\text{Al}$  increases. Partitioning of V into pyroxene at relatively high  $f_{\text{O}_2}$  conditions (i.e., Earth and Mars) increases with increasing Na and  $^{\text{IV}}\text{Al}$ , which provide charge balance for incorporation of  $\text{V}^{4+}$ . Because of the above complexities, a V-valence oxybarometer as measured in planetary pyroxene grains is not likely to be robust.

**Keywords:** Vanadium, pyroxene, planetary basalts, partitioning, SIMS, microprobe

### INTRODUCTION

Comparative planetary mineralogy studies (e.g., Dymek et al. 1976; Papike and White 1979; Papike 1980) began in the late 1970s and early 1980s as a supplement to the many bulk-rock comparative planetology studies being done at the same time (e.g., Consolmagno and Drake 1977; Papike and Bence 1978; Stolper 1979; Bence et al. 1980, 1981; BVSP 1981). The comparative bulk-rock studies work under the philosophy that basalts are probes of planetary interiors, and thus have compositions that reflect the origin and evolution of a planetary body. Such studies can then be used to understand differences among basalt systems, and the influences of a planetary environment on a basalt system. Other workers added a slight variation to this approach and recognized that the compositions of the silicate phases in planetary basalts should also reflect the differing chemical and physical conditions of the melts from which they crystallized, and therefore planetary mineralogy studies should be a viable

way to compare planetary bodies and processes. The first rigorous study that compared basaltic silicate mineral compositions from several planetary bodies (Papike 1981) showed that these minerals indeed held chemical signatures that could be linked to planetary processes and parentage. These conclusions were added to and reinforced in Papike (1998) and new data were added from the now recognized martian basalts in the world's meteorite collections.

Recent comparative planetary mineralogy studies (Karner et al. 2003, 2004; Papike et al. 2004) have added trace-element chemistry to the comparison and have shown that elemental signatures in olivine, plagioclase, and chromite from planetary basalts are affected by the initial volatile-element depletions and enrichments of a planet, basaltic source compositions, crystallization sequence and kinetics, and oxygen fugacity. Elemental systematics in planetary olivine and plagioclase grains also reflect the different styles of igneous differentiation on the planets, and more specifically, the different tectonic settings within and among the planets. The latest comparative planetary mineralogy review (Papike et al. 2005) showed that partitioning of elements with

\* E-mail: jkarner@unm.edu

multiple valence states into planetary pyroxene, olivine, and spinel is affected greatly by oxygen fugacity. Through all of these studies, it has become abundantly clear that basaltic minerals record information not only about their particular igneous setting and process history, but often they carry distinct elemental signatures that can be linked to their planetary parentage. Furthermore, these planetary parentage signatures in minerals are recognizable despite significantly different magmatic and crystallization histories of the host basalts. This is important because many present and future samples (Zolensky et al. 2000) from extraterrestrial planetary soils or regoliths are collections of disaggregated minerals, and may not represent bulk-rock compositions. These “regolith” samples will have key information recorded in individual minerals, and this information can tell us not only about the source region of the rocks, but also about the planetary body as a whole. We believe comparative planetary mineralogy studies will help guide future sample return requirements for scientific study, and will continue to contribute to a database with which present and future planetary (basalt) samples can be compared (Papike 1998).

This comparative planetary mineralogy paper examines the major- and minor-element compositions of planetary pyroxene as well as V partitioning. Although we realize planetary pyroxene chemistry has been examined rigorously before (e.g., Papike 1981), we believe the present study will add to and help refine the conclusions drawn previously because (1) all of these data are new and have been collected in one laboratory by one operator under the same conditions to ensure consistency of analysis; (2) we now have several martian basalts (martian meteorites) to include in this study, whereas Papike (1981) examined only one martian basalt (Shergotty) and, at that time, its martian parentage was not realized; and (3) we have important new data and insight into the systematics of V in planetary pyroxene.

### SAMPLE SUITES

The samples chosen for pyroxene analysis include thin sections from fourteen basalt suites from the Earth, Moon, Mars, and Vesta. The basalts are characteristically fine-grained, and have been affected minimally by crystal accumulation or fractionation. An effort was made to study only basaltic samples that represent liquids, but this was not usually possible. Furthermore, thin sections of specimens that approached the most primitive melts were chosen from each suite, but few were primary.

The terrestrial samples are from five suites differing in tectonic and temporal settings including pre-Tertiary continental flood basalts (Keweenaw-Minnesota), Tertiary continental flood basalts (Columbia Plateau), continental rift basalts (Taos Plateau), oceanic intraplate basalts (Hawaii), and island arc basalts (Papua-New Guinea). Six lunar mare suites from the Apollo (AP) missions include the AP12 Olivine, AP12 Ilmenite, AP12 Pigeonite, AP15 Olivine, and AP15 Pigeonite basalts. The last suite from the Moon includes two KREEP basalts from the AP15 site. Martian samples include two types of basaltic shergottite meteorites. Shergotty and QUE 94201 are classified as basaltic shergottites or pyroxene-phyric basalts, whereas DaG 476, NWA 1110, NWA 1195, and Yamato 980459 (Y98) are olivine-phyric shergottite basalts (Goodrich 2002). Pasamonte, an achondrite meteorite (eucrite), is basalt from the asteroid

Vesta that is relatively unmetamorphosed (unequilibrated). Pasamonte is the only asteroidal basalt in this study, but its mineralogy, chemistry, and igneous evolution is quite representative of unequilibrated eucrites (Pun and Papike 1996). Further information about the sample suites, thin sections, and rock types is given in Table 1, along with appropriate references containing more complete reviews on the basalt suites.

### ANALYTICAL APPROACH

The pyroxene analyses in this paper are new data; all collected using the electron microprobe (EMP) and Secondary Ion Mass Spectrometer (SIMS) at the Institute of Meteoritics. Data collection under identical analytical conditions and standardization ensures consistency of analyses and better constrains trends recognized through other comparative planetary mineralogy studies.

Pyroxene grains in thin sections from 27 samples were analyzed using a JEOL JXA 8200 EMP to determine their major- and minor-element compositions. Pyroxene analyses were made using an accelerating voltage of 15 kV, a beam current of 20 nA, and a beam diameter of 1  $\mu\text{m}$ . Wavelength-dispersive spectrometer counting times of 20 s were used for major elements and 30 s for minor elements, and all data were reduced using a ZAF correction program. Ferric iron was estimated for each analysis using the method described by Droop (1987). For a pyroxene EMP analysis to be deemed acceptable (Schweitzer et al. 1979), it had to meet the following criteria: (1) the total oxide sum =  $100 \pm 2$  wt%; (2) the sum of the tetrahedral site cations, which includes Si and  $^{18}\text{Al}$ , equals  $2 \pm 0.02$  atoms per six O atoms; (3) octahedral cations in the M1 (Mn,  $\text{Fe}^{2+}$ ,  $\text{Fe}^{3+}$ , Mg, Ti, Cr,  $^{18}\text{Al}$ ) and M2 (Ca, Na) site sum to  $2.0 \pm 0.02$ ; and (4) the charge-balance equation [ $^{18}\text{Al} + ^{16}\text{Fe}^{3+} + ^{52}\text{Cr}^{3+} + 2\text{Ti}^{4+} = ^{18}\text{Al} + \text{M}^{2+}\text{Na}$ ] balances to within 0.03 charge. The detection limits reported are defined as three times the standard deviation based on counting statistics.

Vanadium concentrations were measured in pyroxene grains using a Cameca ims 4f SIMS. Analyses were made using a primary beam of O<sup>-</sup> ions accelerated through a nominal potential of 10 kV. A primary beam current of 15 nA yielded a beam size of  $\sim 15$   $\mu\text{m}$ . Sputtered secondary ions were energy filtered using an offset voltage of 105 V and an energy window of  $\pm 25$  V to reduce isobaric interferences. Repeated cycles of peak counting on  $^{51}\text{V}^+$  yielded intensities that were normalized using the relationship of  $^{51}\text{V}^+ / ^{30}\text{Si}^+$  ratios (normalized to the previously measured pyroxene  $\text{SiO}_2$  content). Normalized intensities were then regressed to absolute concentration using a set of pyroxene standards that included KAUG (Mason and Allen 1973), and DW/K1-OPX, DW/K1-CPX. The resulting calibration curve had a correlation coefficient of  $\sim 0.98$ .

Both EMP and SIMS measurements were taken from core to rim on unaltered pyroxene grains, avoiding late-stage and/or groundmass grains. Optical and back-scattered electron (BSE) imaging was used to locate unaltered pyroxene for analyses and to avoid inclusions in target grains. In addition, all SIMS analyses were performed at points previously analyzed by EMP, which helped eliminate inclusion of contaminating phases in the analyses, and also ensured precise  $\text{SiO}_2$  concentrations used to calculate trace element concentrations by SIMS.

### RESULTS AND DISCUSSION

Of the major minerals in basaltic rocks, pyroxene is the most chemically complex, but also probably the most powerful in its ability to record the evolutionary history of a crystallizing basaltic melt (e.g., Bence and Papike 1972). This is because pyroxene is the most important mineral volumetrically in the majority of basalts, it often crystallizes early in a cooling magma, and most importantly, it can incorporate most major and minor elements into its structure except K. For example, Ca, Na, Mn,  $\text{Fe}^{2+}$ , and Mg are accommodated into the 6- to 8-coordinated M2 site; Mn,  $\text{Fe}^{2+}$ ,  $\text{Fe}^{3+}$ , Mg,  $\text{Cr}^{3+}$ ,  $\text{Ti}^{4+}$ , and Al substitute into the 6-coordinated M1 site; and Al, Si, and sometimes  $\text{Fe}^{3+}$  occupy the tetrahedral site.

In this study, we are most concerned with elemental trends in pyroxene that allow for planetary comparisons. These elemental trends reflect planetary influences on the host basalts, best illustrated by the systematics of Ca, Mg, Mn,  $\text{Fe}^{2+}$ ,  $\text{Fe}^{3+}$ , Na,  $\text{Cr}^{3+}$ , and

**TABLE 1.** Basalt suites chosen for pyroxene analysis, along with corresponding setting, locality, thin-section name/number, and rock type

Sample Suite	Geological/Tectonic Setting	Locality	Thin section-Rock Type	References
Continental rift basalts (BVSP*-Taos Plateau)	Extensional tectonics within continental plates	Taos Plateau, New Mexico	TP-15, TP-21 Basaltic andesites	Dungan et al. 1981
Island Arc basalts (BVSP-Island Arc)	Ocean floor volcanism at convergent plate boundaries	New Britain, Papua-New Guinea	IA-1, IA-7 Porphyritic basalts	Taylor et al. 1981
Oceanic Intraplate basalts (BVSP-Hawaiian)	Oceanic-island hotspot volcanism	Hawaiian islands	HAW-17 Ankaramite	Bence 1981
Continental flood basalts (BVSP-Keweenawan and Columbia Plateau)	Flood lavas produced at continental rifts	Keweenawan, Lake Superior Basin, N. America; Columbia Plateau, Washington	KEW-1 Olivine tholeiite KEW-13 Weakly Alkaline basalt CP-4 Olivine basalt CP-8 Porphyritic basalt	Green and Haskin 1981 Haggerty and Irving 1981
Lunar Basalts	Lunar mare basaltic volcanism	Apollo 11, 12, 15 and 17 landing sites	12020, 12075, 15016, 15545 Olivine basalts; 12022, 12063 Ilmenite basalts; 12021, 12052, 15499, 15058 Pigeonite basalts; 15382, 15386 KREEP basalts;	Papike et al. 1976
Martian Basalts	Martian basaltic volcanism	Martian meteorites	Shergotty, QUE94201 Pyroxene-phyric basalts; DaG476, NWA1110, NWA1195, Y980459 Olivine-phyric basalts	McSween and Treiman 1998; Meyer 2003
Asteroidal (4 Vesta) basalts	Basaltic volcanism on asteroidal bodies	Eucrite meteorites from asteroid 4 Vesta	Pasamonte, Unequilibrated eucrite	Takeda et al. 1976

\* BVSP = Basaltic Volcanism Study Project

**TABLE 2.** Average composition of pyroxene from planetary basalt suites

Suite	Keweenawan N = 75	Island Arc N = 55	Columbia Plateau N = 62	Hawaiian N = 37	Taos Plateau N = 61	Mars N = 235	AP 12 Ilmenite N = 66	AP 12 Pigeonite N = 58	AP 12 Olivine N = 82	AP 15 Olivine N = 56	AP 15 Pigeonite N = 75	AP 15 KREEP N = 62	4 Vesta N = 35
SiO <sub>2</sub> wt%*	51.7	52.4	52.0	50.6	51.6	52.6	47.9	49.7	51.1	50.8	51.3	52.8	51.0
Al <sub>2</sub> O <sub>3</sub>	1.92	2.58	2.12	3.58	3.26	0.86	4.47	3.20	2.59	1.61	2.30	2.20	1.55
Fe <sub>2</sub> O <sub>3</sub>	1.44	1.37	1.63	2.24	3.12	0.14	0.00	0.00	0.00	0.00	0.00	0.00	0.00
TiO <sub>2</sub>	0.95	0.54	0.79	1.03	0.66	0.27	2.70	1.34	1.07	0.85	0.70	0.78	0.23
Cr <sub>2</sub> O <sub>3</sub>	0.27	0.29	0.15	0.51	0.13	0.47	0.75	1.03	0.88	0.53	0.97	0.89	0.89
MgO	15.7	17.4	17.6	16.2	19.7	19.2	13.2	16.2	18.8	15.5	17.8	25.0	16.6
FeO	8.76	6.61	10.1	3.89	9.15	19.5	15.3	18.3	17.1	22.7	18.2	14.6	24.8
MnO	0.24	0.22	0.29	0.12	0.31	0.62	0.27	0.33	0.32	0.36	0.31	0.24	0.84
CaO	18.9	19.1	15.8	21.3	12.7	6.4	15.3	10.3	8.26	8.37	9.12	3.32	5.07
Na <sub>2</sub> O	0.29	0.19	0.19	0.27	0.33	0.07	0.05	0.02	<0.02	<0.02	0.03	0.02	<0.02
Total	100.2	100.7	100.6	99.7	101.0	100.1	99.9	100.4	100.0	100.8	100.7	99.8	101.0
Formula proportions based on 6 O atoms													
Si	1.918	1.913	1.914	1.865	1.879	1.970	1.821	1.876	1.906	1.932	1.916	1.920	1.939
Al	0.084	0.111	0.092	0.156	0.140	0.038	0.200	0.142	0.114	0.072	0.101	0.094	0.069
Fe <sup>3+</sup>	0.040	0.038	0.045	0.062	0.086	0.004	0.000	0.000	0.000	0.000	0.000	0.000	0.000
Ti	0.026	0.015	0.022	0.029	0.018	0.008	0.077	0.038	0.030	0.024	0.020	0.021	0.007
Cr	0.008	0.008	0.004	0.015	0.004	0.014	0.022	0.030	0.026	0.016	0.028	0.026	0.027
Mg	0.870	0.945	0.965	0.890	1.062	1.058	0.747	0.903	1.043	0.874	0.983	1.348	0.936
Fe <sup>2+</sup>	0.272	0.203	0.313	0.120	0.277	0.620	0.488	0.580	0.534	0.727	0.571	0.447	0.793
Mn	0.008	0.007	0.009	0.004	0.009	0.020	0.009	0.010	0.010	0.012	0.010	0.007	0.027
Ca	0.753	0.747	0.622	0.841	0.501	0.259	0.624	0.419	0.331	0.342	0.368	0.133	0.208
Na	0.021	0.013	0.013	0.019	0.024	0.005	0.004	0.002	0.001	0.001	0.002	0.002	0.001
Total	4.000	4.000	4.000	4.000	4.000	3.996	3.992	4.001	3.995	4.000	4.000	3.999	4.006
Wo	39.7	39.4	32.8	45.4	27.6	13.4	33.7	22.2	17.4	17.6	19.3	6.9	10.8
En	45.9	49.8	50.7	48.1	57.5	54.5	40.1	47.4	54.6	45.0	51.0	69.9	48.3
Fs	14.3	10.8	16.5	6.5	15.0	32.1	26.1	30.4	28.0	37.4	29.7	23.2	40.9
Fe/Fe+Mg	0.24	0.17	0.24	0.12	0.20	0.38	0.39	0.39	0.34	0.46	0.38	0.26	0.46
Vanadium concentrations in ppm													
	N = 15			N = 11		N = 73		N = 15		N = 36		N = 20	
V (ppm)†	527 (12)			213 (6)		198 (5)		397 (9)		283 (7)		130 (3)	
Vanadium bulk rock concentration in ppm													
	470			345		162		170		200		60	

Notes: Vanadium bulk rock concentrations from BVSP (1981) for Keweenawan and Hawaiian; Haskin and Warren (1991) for AP12 and AP15 rocks; Meyer (2003) for Shergotty, DaG476, and NWA1110; Shirai and Ebihara (2004) for Y98; and Wänke et al. (1977) for Pasamonte.

\* Electron microprobe analyses have typical errors of 3% for major elements and up to 5% for minor and trace elements.

† V (ppm): analyses by SIMS; errors shown in parantheses are ~3% based on machine precision and counting statistics.

V in pyroxene, and these will be presented in the text. Average pyroxene EMP and SIMS compositional data for the 14 basalt

suites are presented in Table 2, but analyses representing the compositional range for the suites (coded by thin section) are

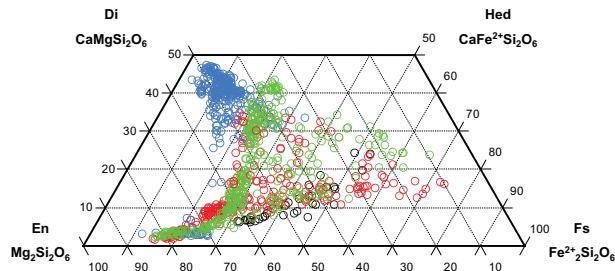


FIGURE 1. Pyroxene Di ( $\text{CaMgSi}_2\text{O}_6$ )-Hed ( $\text{CaFeSi}_2\text{O}_6$ )-En ( $\text{Mg}_2\text{Si}_2\text{O}_6$ )-Fs ( $\text{Fe}_2\text{Si}_2\text{O}_6$ ) composite variation diagram for all pyroxene analyses from the Earth (blue), Moon (green), Mars (red), and Vesta (black).

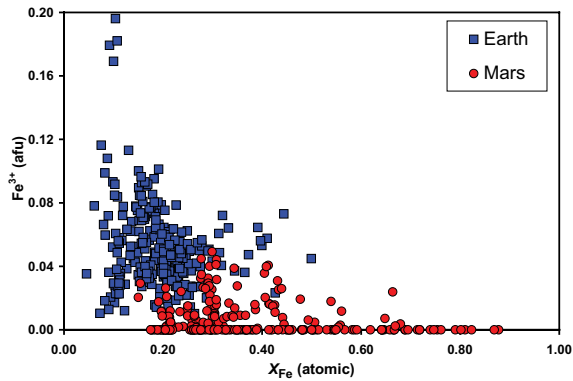


FIGURE 2.  $\text{Fe}^{3+}$  atoms per 6-oxygen formula unit (afu) vs.  $X_{\text{Fe}}$  [ $(\text{Fe}/(\text{Fe}+\text{Mg}))_{\text{atomic}}$ ] variation diagram for terrestrial and martian pyroxene.

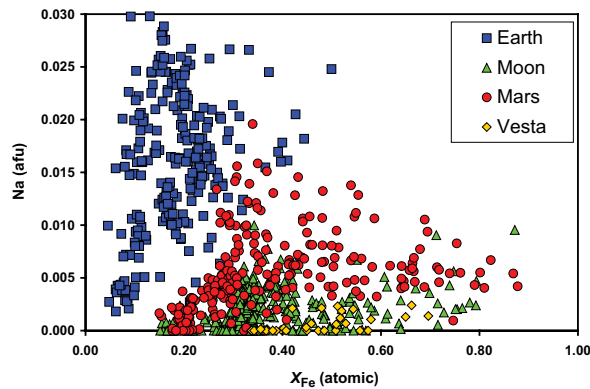


FIGURE 3. Na (afu) vs.  $X_{\text{Fe}}$  for pyroxene grains from the four different planetary bodies.

presented in Appendix Table 1 on the AmMin web site.<sup>1</sup> The appendix also contains figures A1–A8, which include all pyroxene

<sup>1</sup> Deposit item AM-06-028, Appendix Table and Appendix Figures A1–A8, which present analyses representing the compositional range for the suites (coded by thin section). Deposit items are available two ways: For a paper copy contact the Business Office of the Mineralogical Society of America (see inside front cover of recent issue) for price information. For an electronic copy visit the MSA web site at <http://www.minsocam.org>, go to the American Mineralogist Contents, find the table of contents for the specific volume/issue wanted, and then click on the deposit link there.

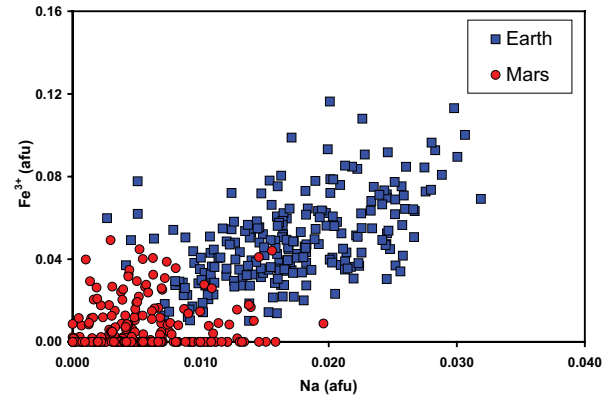


FIGURE 4.  $\text{Fe}^{3+}$  (afu) vs. Na (afu) for pyroxene grains from Mars and Earth. The positive correlation between  $\text{Fe}^{3+}$  and Na shows that the charge-balance substitutional couple of  $^{\text{M}2}\text{Na}^{\text{M}1}\text{Fe}^{3+}$  is very important in terrestrial pyroxenes.

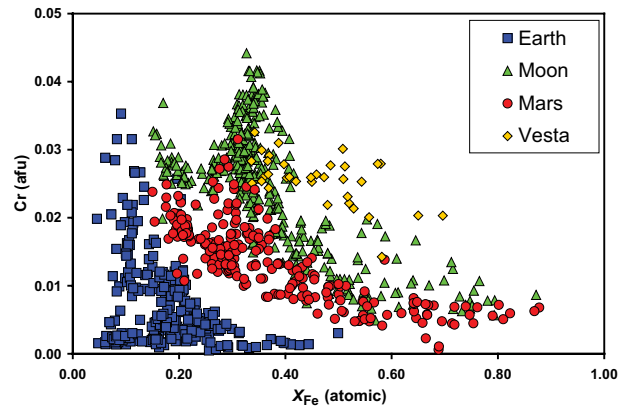


FIGURE 5. Cr vs.  $X_{\text{Fe}}$  for pyroxene grains from the Earth, Moon, Mars, and Vesta.

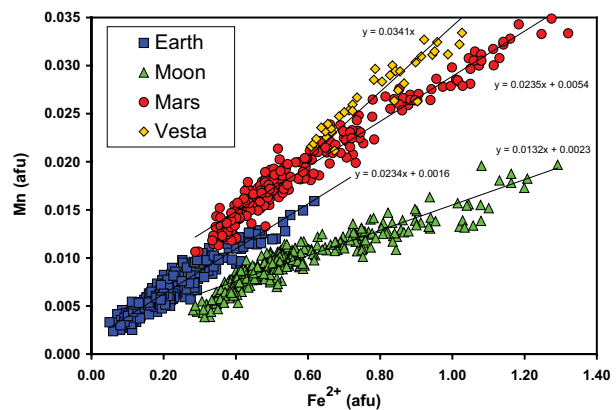


FIGURE 6. Mn vs.  $\text{Fe}^{2+}$  in atoms per 6-oxygen formula unit (afu) for pyroxene analyses from the Earth, Moon, Mars and Vesta. Best-fit trend lines are indicated and their equations are given.

analyses broken down by thin section for the systematics of  $\text{Fe}^{3+}$  vs.  $X_{\text{Fe}}$ , Na vs.  $X_{\text{Fe}}$ , Cr vs.  $X_{\text{Fe}}$ , Mn vs.  $X_{\text{Fe}}$ ,  $V^*$  vs.  $X_{\text{Fe}}$ ,  $V^*$  vs. Ca, Ti vs.  $X_{\text{Fe}}$ , and Al vs.  $X_{\text{Fe}}$ , where  $X_{\text{Fe}} = \text{Fe}/(\text{Fe} + \text{Mg})_{\text{atomic}}$ . The entire data set is available to any interested parties by request from the first author.

### Pyroxene quadrilateral (Quad) element systematics

Some of the major features of the “Quad” chemical systematics of planetary pyroxene grains are illustrated in Figure 1. Pyroxenes from the Earth show the most Mg-rich and Ca-rich compositions, and also show the least degree of Fe-rich enrichment compared with the other planets. The small degree of Fe-enrichment in the terrestrial pyroxenes is a consequence of sample selection, as we chose to use the same suites as were used in the Papike (1981) BVSP paper, and in several other comparative planetary mineralogy studies (e.g., Karner et al. 2003, 2006). The lunar and martian pyroxene grains show a large chemical variation in which zoning extends to the very Fe-rich compositions, and also includes the pyroxenoid pyroxferroite (not studied here, e.g., Aramovich et al. 2002). Lunar and martian pyroxenes also show both low- and high-Ca trends that zone to more Fe-rich compositions, and thus we infer that these compositions are fairly representative of pyroxene grains from those planets. Pasamonte pyroxenes show only a low-Ca trend, but again the pyroxenes from this sample have been proven to be quite characteristic of those from unequilibrated eucrite basalts (Pun and Papike 1996).

### Fe<sup>3+</sup> systematics

Figure 2 is a plot of Fe<sup>3+</sup> in atoms per 6-oxygen formula unit (afu) vs.  $X_{\text{Fe}}$  of pyroxene grains from Earth and Mars. The parameter  $X_{\text{Fe}} = \text{Fe}/(\text{Fe} + \text{Mg})_{\text{atomic}}$  is used here and in several following diagrams to indicate the fractionation sequence. The plot shows that terrestrial pyroxene contains significantly more Fe<sup>3+</sup> than pyroxene from Mars (see also Table 2). Pyroxene grains from the Moon and Vesta contain almost no Fe<sup>3+</sup> and thus are not included in the plot. The amount of Fe<sup>3+</sup> in pyroxene can be related directly to the oxygen fugacity at which the host basalts crystallized. Basalts on the Earth crystallize within approximately 1 or 2 log units of the Quartz-Fayalite-Magnetite (QFM) buffer (e.g., Ballhaus 1993), and thus a significant portion of the Fe in terrestrial melts is oxidized to Fe<sup>3+</sup>, and this is reflected in the composition of the pyroxene that crystallizes from these melts. Martian basalts crystallize at a range of  $f_{\text{O}_2}$  conditions from approximately the Iron-Wustite (IW) buffer up to the QFM buffer (Wadhwa 2001; Herd et al. 2001; Herd 2003; McCanta et al. 2004). Therefore, martian pyroxene grains show a range of Fe<sup>3+</sup> from zero to only about a third of the Fe<sup>3+</sup> that is contained in the most oxidized terrestrial samples. Lunar and Vestan basalts crystallize at conditions of approximately IW-1, or QFM-4.5, (e.g., Sato et al. 1973; Stolper 1977; Jones 2004; Karner et al. 2006), where all of the Fe has been reduced to Fe<sup>2+</sup> or Fe metal, and there is no Fe<sup>3+</sup>.

### Na systematics

The variability of Na in the planetary pyroxene grains is shown in Figure 3. Terrestrial pyroxene shows a large variation and also the highest concentration of Na compared with pyroxene from the other three planetary bodies. These terrestrial trends are largely due to the fact that high-Ca pyroxenes have much higher Na than do low-Ca pyroxenes (Papike 1998) and higher Fe<sup>3+</sup> in terrestrial basalts allows more acmite (NaFe<sup>3+</sup>Si<sub>2</sub>O<sub>6</sub>) component substitution. In addition, most of the terrestrial pyroxene grains are from basaltic magmas that have interacted with continental

crust. Continental rift (Taos Plateau) and continental flood (Ke-weenawan, Columbia Plateau) basalts are known to be enriched in incompatible elements compared with ocean-floor and island-arc basalts, and this is most likely caused by assimilation of crustal materials (BVSP 1981; Hess 1989). These incompatible element enrichments are also recorded in plagioclase from these basalts (Karner et al. 2003), and now these enrichments also are noted in pyroxenes. In contrast to the terrestrial data, pyroxene from Vesta and the Moon contain very little Na. This is consistent with the volatile-depleted nature of the parent bodies. Depletions in volatile Na and K also have been noted in plagioclase from Vesta and the Moon (Papike 1998, Karner et al. 2003). Pyroxenes from martian basalts show higher Na contents than pyroxene from Vesta and the Moon, but generally less Na than pyroxene from the Earth. Higher Na in terrestrial pyroxene compared with martian pyroxene could be a consequence of higher  $f_{\text{O}_2}$  for Earth than Mars, which produces more Fe<sup>3+</sup> that in turn goes into terrestrial pyroxene. This Fe<sup>3+</sup> (in the M1 site) is available to charge balance Na (in the M2 site) as the acmite component in pyroxene (Fig. 4). Important charge-balance couples for planetary pyroxenes are thoroughly discussed in Papike (1981) and Papike et al. (2006).

### Cr systematics

Figure 5 is a plot of Cr vs.  $X_{\text{Fe}}$  for pyroxene from the four different planetary bodies. Pyroxenes from all the planets are similar in that Cr concentrations decrease with increasing  $X_{\text{Fe}}$ . This is the expected trend for a compatible element with increasing fractionation or crystallization. The plot also shows that pyroxene from the Moon is only slightly enriched in Cr compared with pyroxenes from the other planetary bodies, even though Cr contents in lunar melts are higher. This is different from what is recorded in olivine from mare basalts, where Cr concentrations are up to 7 times greater than in terrestrial and martian olivine (Karner et al. 2003). This difference between the relative Cr contents of lunar olivine and pyroxene reflects the fact that Cr in lunar basaltic melts is largely Cr<sup>2+</sup>, which partitions into olivine, whereas Cr<sup>3+</sup> in lunar melts partitions into pyroxene (Sutton et al. 1993). The Cr<sup>3+</sup> activity of lunar melts, then, is similar to the Cr<sup>3+</sup> activity of terrestrial and martian melts.

### Mn-Fe systematics

Figure 6 shows that pyroxene grains from the different bodies have distinct Mn/Fe<sup>2+</sup> ratios in the order of Vesta > Mars > Earth > Moon. The trend of Mn/Fe<sup>2+</sup> ratios increasing with heliocentric distance (except for the Moon, which can be explained by the impactor formation model) has been documented previously in both pyroxene and olivine (Papike 1998; Papike et al. 2003). Manganese enrichments in the bulk compositions of Vesta and Mars compared with the Earth and Moon also have been noted (Drake et al. 1989). One interpretation is that the distinct Mn/Fe<sup>2+</sup> trends are best explained as the result of an early, pre-accretional heating event in the inner solar system. This heating event would have depleted the inner solar system planetesimals in volatile elements relative to the outer planetesimals, and is supported by the observed depletion of volatile K relative to refractory U in the Earth and Moon compared with Vesta and Mars (Taylor 1992). Therefore, planetary differences in Mn/Fe ratios are most

likely due to the fact that Mn is much more volatile than Fe, and outer bodies preserved more Mn relative to Fe, than did bodies closer to the Sun. Thus, differences in Mn/Fe ratios are the result of initial accretional abundances and accretional position in the solar system. If this is true, then one would expect lunar and terrestrial pyroxene to have similar ratios if they formed at approximately the same heliocentric distance in the solar system, as suggested by oxygen isotope data (Clayton et al. 1976). Terrestrial pyroxene, however, has systematically higher Mn/Fe than lunar pyroxene. Low Mn/Fe ratios in lunar silicates are consistent with the overall volatile depletion of the Moon, and also with the “giant impact hypothesis” for the origin of the Moon, wherein the Moon accreted from a hot, volatile-depleted debris ring around the early Earth.

Although this explanation for differing Mn/Fe ratios may not be totally correct, several studies have shown that basaltic silicate minerals preserve this relationship (Dymek et al. 1976; Papike 1998; Karner et al. 2003), and so it can be used as a fingerprint of planetary basalt parentage (e.g., Papike et al. 2003). The data in Figure 6 add to those from previous studies and help to define precisely the Mn/Fe ratios of pyroxene from the Earth, Moon, Mars, and Vesta because they were all collected in the same laboratory under identical analytical conditions and standardization.

### V systematics in pyroxene

As part of the initiative of the Lunar and Planetary Institute and the NASA Cosmochemistry Program “Oxygen in the Solar System,” we have been developing V valence oxybarometers (VVOs), as measured in basaltic phases. Vanadium can exist as  $V^{2+}$ ,  $V^{3+}$ ,  $V^{4+}$ , and  $V^{5+}$  (Canil 1997, 1999), and VVOs can record at least 8 orders of magnitude in  $f_{O_2}$ , allowing for applicability to both oxidized and reduced magmas from planetary bodies. The applicability at low  $f_{O_2}$  conditions is especially important because traditional  $Fe^{2+}/Fe^{3+}$  barometers are ineffectual here since there is no  $Fe^{3+}$  present in these environments. Our first VVO work concentrated on basaltic glasses (Sutton et al. 2005; Karner et al. 2006), but now workers are developing VVOs for spinel (Papike et al. 2004; Righter et al. 2004), olivine (Sutton and Newville 2005; Shearer et al. 2006) and pyroxene (Papike et al. 2005). A VVO for pyroxene would be particularly germane to the study of some martian and asteroidal basalts (i.e., eucrites) because pyroxene is often the first phase to crystallize from these melts.

Table 3 summarizes some of the predictions for substitutional couples for V as a function of  $f_{O_2}$  and planet type (e.g., volatile-depleted Moon) of Papike et al. (2005). Papike et al. (2005) concluded correctly, based on limited data, that substitutional couples involving  $V^{3+}$  are more compatible in pyroxene than those involving  $V^{4+}$ . In the following section, we examine the partitioning behavior of V in pyroxenes from planetary basalts further in an attempt to evaluate better the potential for a quantitative pyroxene VVO.

To evaluate the partitioning of V in pyroxene, we collected V data (by SIMS) on a set of representative samples from the four different bodies. The samples chosen for V analysis included KEW-1 and HAW-17 from Earth; Shergotty, QUE94201 (QUE), and Y98 from Mars; 12075, 15058, and 15499 from the Moon; and Pasamonte from Vesta. The selected samples from each

**TABLE 3.** Substitutions of V in pyroxene as a function of  $f_{O_2}$

Moon- Vesta: IW-1	$f_{O_2}$ range for planetary basalts	
	Mars: IW to IW+2	Earth: IW+2 to IW+6
Vanadium valences in basaltic melts		
$V^{2+} > V^{4+}$ , low $V^{2+}$	$V^{4+} = V^{3+}$	$V^{4+} > V^{3+}$ , $V^{5+}$
Pyroxene charge balance couples = “others”		
none	$M^2Na^{M^1V^{4+} - IVAl}$	$M^2Na^{M^1V^{4+} - IVAl}$
low	$M^1V^{4+} - 2^{IVAl}$	$M^1V^{4+} - 2^{IVAl}$
none	$M^2Na - M^1V^{3+}$	low
$M^1V^{3+} - IVAl$	low	none
$V^{2+}$ for Ca, Mg, $Fe^{2+}$	none	none

Notes: Vanadium valences present in basaltic melts on the different planets plus the most important charge couples for V cations in planetary pyroxene grains. After Papike et al. 2005.

planet show a range of pyroxene quadrilateral compositions, which allows us to evaluate V partitioning as a function of both pyroxene Ca-content and increasing fractionation. The quadrilateral compositions of the pyroxene grains from the selected samples are shown in Figure 7, and we used these data to select our SIMS points for V analysis.

At this point, we would like to state that the discussion of partition coefficients ( $D$ -values) for complex silicates has been oversimplified in much of the published literature. It is not sufficient, for example, to talk about  $D_{V^{3+}}$  or  $D_{V^{4+}}$ . We must describe the  $D$  of the substitutional couple. For example, Fowler et al. (1994) showed that the order of compatibility for Al in diagenetic pyroxene is  $M^1Cr - IVAl > M^1Al - IVAl > M^1Ti - 2^{IVAl}$ . The same logic must be used for V, and thus the complexity.

Figures 8a and 8b illustrate  $X_{Fe}$  and Ca content in pyroxene grains vs.  $V_{pyroxene}/V_{rock}$ . Here, we use the measured V in pyroxene and normalize to literature values of V in the bulk rock, and call this value  $V^*$ . The parameter  $V^*$  is not a true  $D$ -value because some of these basalts are not melts but cumulates and, in addition, even if the bulk-rock composition represents a melt, only the core composition of a pyroxene that is the first phase on the liquidus gives a good  $D$  approximation. Thus  $V^*$  does not represent the equilibrium distribution of V between pyroxene and the coexisting melt. However, its use “levels the playing field” to account for the relative abundance of V in the differing melts. Only the most Mg-rich pyroxene compositions are relevant as  $D$ -value approximations, but we include more Fe-rich analyses (up to  $X_{Fe} = 0.4$ ) to illustrate V partitioning with increasing fractionation.

Figure 8a shows that at the lowest  $X_{Fe}$  for each planet, (i.e., the cores of the pyroxene grains),  $V^*$  values are highest in pyroxene grains from Vesta and the Moon, and are lower and variable in terrestrial and martian pyroxene, although QUE pyroxene (martian) actually shows the highest  $V^*$ . The figure also shows that V partitioning decreases with increasing  $X_{Fe}$  of the pyroxene in Pasamonte and QUE. This is because in these basalts, pyroxene and plagioclase co-crystallize and plagioclase depletes the melt in Al and thus the available  $^{IV}Al$  needed for  $V^{3+}$  substitution (i.e.,  $M^1V^{3+} - IVAl$ ). However, in lunar rocks 15058 (slower cooled) and 15499 (faster cooled), plagioclase crystallization is delayed and thus the activity of Al in the melt increases and more Al is incorporated into the crystallizing pyroxene, which enables a higher  $V^*$ . After plagioclase crystallizes,  $V^*$  decreases. Figure 8b shows that the Ca content of planetary pyroxene has little direct

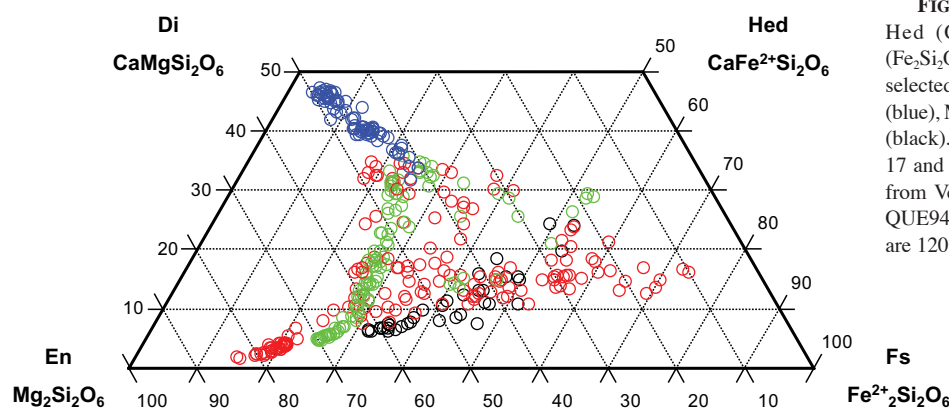


**FIGURE 7.** Pyroxene Di ( $\text{CaMgSi}_2\text{O}_6$ )-Hed ( $\text{CaFe}^{2+}\text{Si}_2\text{O}_6$ )-En ( $\text{Mg}_2\text{Si}_2\text{O}_6$ )-Fs ( $\text{Fe}_2\text{Si}_2\text{O}_6$ ) composite variation diagram for selected pyroxene analyses from the Earth (blue), Moon (green), Mars (red), and Vesta (black). Terrestrial samples include HAW-17 and KEW-1; Pasamonte is the sample from Vesta; Mars samples are Shergotty, QUE94201, and Y98, and lunar samples are 12075, 15499, and 15058.

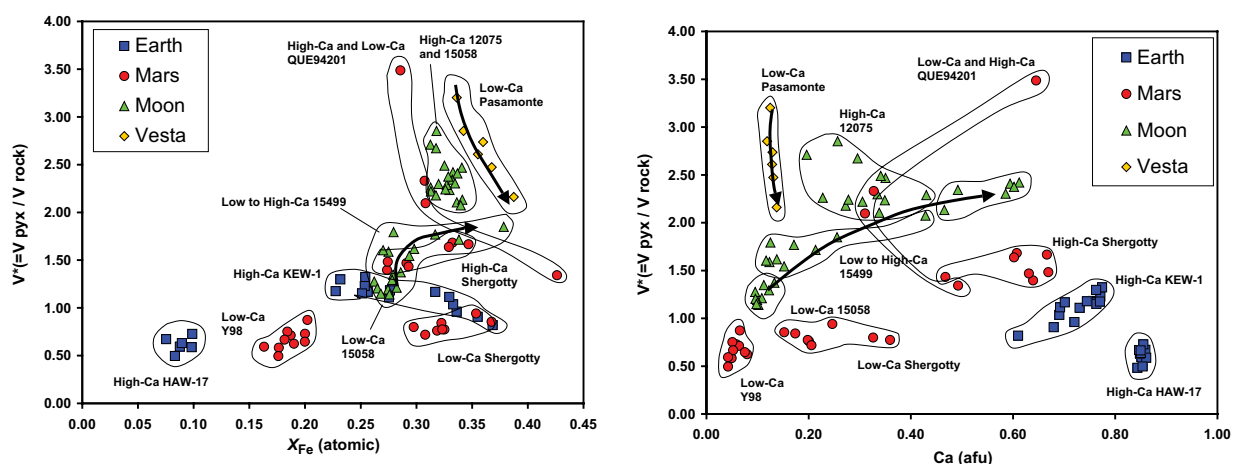


**FIGURE 8.** (a)  $V_{\text{pyroxene}}/V_{\text{rock}} (=V^*)$  vs.  $X_{\text{Fe}}$  for pyroxene grains from select basalt suites from the four different bodies. Labels designate low-Ca and high-Ca pyroxenes from the samples. Bold arrows indicate increasing crystallization trends in Pasamonte and 15499. See text for discussion. (b)  $V^*$  vs. Ca (afu) for the same pyroxene analyses as in Figure 7a. Bold arrows indicate increasing crystallization trends in Pasamonte and lunar pyroxene grains. See text for discussion.

effect on the V partitioning, but it does indirectly. This is because, for example, Na follows Ca into the pyroxene structure. Papike (1981) showed that high-Ca Shergotty pyroxene was also higher in Na. This Na enables a higher  $V^*$  in the pyroxene.

At least three factors influencing V partitioning in pyroxene are (1) the variable  $f_{\text{O}_2}$  conditions of the planets, which determines the  $V^{3+}/V^{4+}$  ratios in basaltic melts; (2) the availability of elements for coupled substitution and charge balance with the dominant V valence cation; and (3) the crystallization sequence in each basalt. For example, low  $f_{\text{O}_2}$  conditions on the Moon and Vesta ( $\sim\text{IW}-1$ ) lead to high  $V^{3+}/V^{4+}$  ratios in basaltic melts. The most important charge-balance couple for  $V^{3+}$  in pyroxene grains from the Moon and Vesta is  $V^{3+}\text{-}^{\text{IV}}\text{Al}$ , because there is little Na in these grains available for charge balance (see Table 3). Therefore, we should see an increase in  $V^*$  with increasing  $^{\text{IV}}\text{Al}$  in both lunar and Vesta pyroxene. This is exactly what we see in Figure 9 for lunar samples 15058 and 15499, and Pasamonte from Vesta. Note the opposite crystallization trends for Moon and Vesta pyroxenes and the additional complexity recorded in pyroxene grains from lunar sample 15058. In 15058, pyroxene starts crystallizing and  $V^*$  increases steadily with increasing

tetrahedral Al. When plagioclase appears on the liquidus, it begins to compete strongly for Al in the melt, as documented by Bence and Papike (1972). Abruptly, the activity of Al in the melt drops off and Al available for substitution into pyroxene with  $V^{3+}$  decreases; subsequently  $V^*$  drops considerably. In the terrestrial and martian case, the same factors affect V partitioning into pyroxene. The relatively high  $f_{\text{O}_2}$  conditions on Mars and Earth lead to low  $V^{3+}/V^{4+}$  ratios in basaltic melts. This leads to  $V^{4+}\text{-}2^{\text{IV}}\text{Al}$  and  $V^{4+}\text{-}^{\text{IV}}\text{Al} + ^{\text{M}2}\text{Na}$  as the most important charge couples in pyroxene grains from these planets (see Table 3). Figure 10 illustrates this feature, where pyroxenes from Mars and Earth show increasing  $V^*$  with increasing Na and tetrahedral Al. Figure 10 also shows that Shergotty pyroxene is affected in a similar manner as pyroxene from lunar sample 15058 (described above). At first, both Shergotty high-Ca and low-Ca pyroxenes crystallize without plagioclase and  $V^*$  increases with increasing crystallization (black arrows). When plagioclase begins to crystallize, Al and Na are much less available to enter pyroxene as charge-balancing substitutional couples with V, and thus  $V^*$  decreases dramatically (red arrow).

The conclusion we can draw from this work is that although

$f_{O_2}$  does have a strong effect on V incorporation into pyroxene, this incorporation is influenced strongly by melt composition and thus crystallization sequence and crystallization kinetics (e.g., delayed plagioclase crystallization). We conclude, as did Papike et al. (2005), that  $V^{3+}$ - $^{IV}Al$  is much more compatible in the pyroxene crystal structure than  $V^{4+}$ - $^{2IV}Al$  or Na-containing couples. However, based on this study, we do not think a pyroxene VVO will be robust.

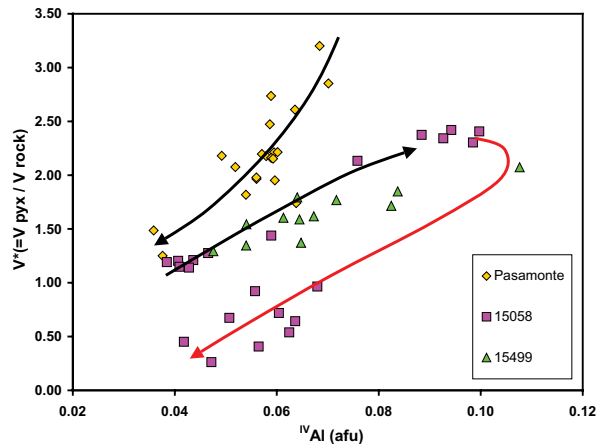


**FIGURE 9.**  $V^*$  vs.  $^{IV}Al$  systematics in pyroxenes from Vesta (Pasamonte) and the Moon. The black arrow for Pasamonte represents pyroxene crystallization trend with co-crystallizing plagioclase. The black arrow for 15499 and 15058 indicates pyroxene crystallization trend before plagioclase crystallization. The red arrow indicates continued crystallization of 15058 after the beginning of plagioclase crystallization. See text for discussion.

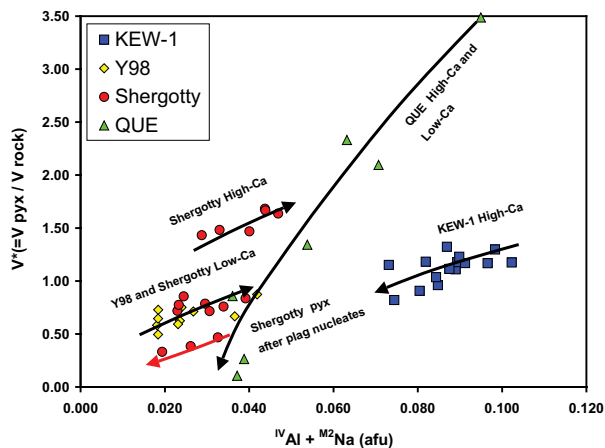


**FIGURE 10.**  $V^*$  vs.  $^{IV}Al + M_2Na$  systematics in pyroxenes from the Earth and Mars. The black arrows for Y98 and Shergotty represent low-Ca and high-Ca pyroxene crystallization trend in the absence of plagioclase. The black arrow for QUE and KEW-1 pyroxene indicates increasing crystallization with co-crystallizing plagioclase. The red arrow indicates crystallization trend of Shergotty pyroxene after the beginning of plagioclase crystallization. See text for discussion.

## CONCLUDING STATEMENT

Comparative planetary mineralogy studies (e.g., Karner et al. 2003, 2004; Papike 1981, 1998; Papike et al. 2003, 2005) show that elemental signatures in minerals from planetary basalts record planetary parentage and processes that affect basaltic magmatism, including igneous setting and differentiation. Studies such as these may be important when dealing with small, unrepresentative bulk samples from regoliths on planetary surfaces to be collected on future planetary sample return missions.

## ACKNOWLEDGMENTS

This research was supported by a NASA Cosmochemistry Grant to J.J.P. and the Institute of Meteoritics. We acknowledge NASA Johnson Space Center and the Smithsonian Institution for providing us with the extraterrestrial and terrestrial basalt thin sections for our studies. We thank Mike Spilde and Paul Burger for their technical assistance with the EMP and SIMS analyses. This manuscript was much improved by the comments and suggestions of reviewers Malcolm Rutherford, Allan Treiman, and Associate Editor David Vaniman.

## REFERENCES CITED

- Aramovich, C.J., Herd, C.K., and Papike, J.J. (2002) Symplectites derived from metastable phases in martian basaltic meteorites. *American Mineralogist*, 87, 1351–1359.
- Ballhaus, C. (1993) Redox states of lithospheric and asthenospheric upper-mantle. *Contributions to Mineralogy and Petrology*, 114, 331–348.
- Bence, A.E. (1981) Oceanic intraplate volcanism. In R.B. Merrill and R. Ridings, Eds., *Basaltic Volcanism on the Terrestrial Planets*, p. 161–192. Pergamon, New York.
- Bence, A.E. and Papike, J.J. (1972) Pyroxenes as recorders of lunar basalt petrogenesis: chemical trends due to crystal-liquid interaction. *Proceedings of the 3<sup>rd</sup> Lunar Science Conference*, 1, 431–469.
- Bence, A.E., Grove, T.L., and Papike, J.J. (1980) Basalts as probes of planetary interiors: constraints on the chemistry and mineralogy of their source regions. *Precambrian Research*, 10, 249–279.
- Bence, A.E., Grove, T.L., Papike, J.J., and Taylor, S.R. (1981) Basalts as probes of planetary interiors: constraints from major and trace element chemistry. In R.B. Merrill and R. Ridings, Eds., *Basaltic Volcanism on the Terrestrial Planets*, p. 311–338. Pergamon, New York.
- BVSP (Basaltic Volcanism Study Project) (1981) *Basaltic Volcanism on the Terrestrial Planets*, 1286 p. Pergamon, New York.
- Canil, D. (1997) Vanadium partitioning and the oxidation state of Archaean komatiite magmas. *Nature*, 389, 842–845.
- (1999) Vanadium partitioning between orthopyroxene, spinel and silicate melt, and the redox states of mantle source regions for primary magmas. *Geochimica et Cosmochimica Acta*, 63, 557–572.
- Clayton, R.N., Onuma, N., and Mayeda, T.K. (1976) A classification of meteorites based on oxygen isotopes. *Earth and Planetary Science Letters*, 30, 10–18.
- Consolmagno, G.J. and Drake, M.J. (1977) Composition and evolution of the eucrite parent body. *Geochimica et Cosmochimica Acta*, 41, 1271–1282.
- Drake, M.J., Newsom, H.E., and Capobianco, C.J. (1989) V, Cr, and Mn in the Earth, Moon, EPB, SPB, and the origin of the moon: experimental studies. *Geochimica et Cosmochimica Acta*, 53, 2101–2111.
- Droop, G.T.R. (1987) A general equation for estimating  $Fe^{3+}$  concentrations in ferromagnesian silicates and oxides from microprobe analyses, using stoichiometric criteria. *Mineralogical Magazine*, 51, 431–435.
- Dungan, M.A., Lipman, P.W., and Williams, S. (1981) Continental rift volcanism. In R.B. Merrill and R. Ridings, Eds., *Basaltic Volcanism on the Terrestrial Planets*, p. 108–131. Pergamon, New York.
- Dymek, R.F., Albee, A.L., Chodos, A.A., and Wasserburg, G.J. (1976) Petrography of isotopically-dated clasts in the Kapoeta howardite and petrologic constraints on the evolution of its parent body. *Geochimica et Cosmochimica Acta*, 40, 1115–1130.
- Fowler, G.W., Papike, J.J., Spilde, M.N., and Shearer, C.K. (1994) Diogenites as asteroidal cumulates: insights from orthopyroxene major and minor element chemistry. *Geochimica et Cosmochimica Acta*, 59, 3071–3084.
- Goodrich, C.A. (2002) Olivine-phyric martian basalts: a new type of shergottite. *Meteoritics and Planetary Science*, 37, B31–B34.
- Green, J.C. and Haskin, L.A. (1981) Pre-Tertiary continental flood basalts. In R.B. Merrill and R. Ridings, Eds., *Basaltic Volcanism on the Terrestrial Planets*, p. 30–77. Pergamon, New York.
- Haggerty, S.E. and Irving, A.J. (1981) Tertiary continental flood basalts. In R.B. Merrill and R. Ridings, Eds., *Basaltic Volcanism on the Terrestrial Planets*, p. 78–107. Pergamon, New York.
- Haskin, L. and Warren, P. (1991) Lunar Chemistry. In G. Heiken, D. Vaniman,

- and B.M. French, Eds., *Lunar Sourcebook*, p. 355–474. Cambridge University Press, Cambridge.
- Herd, C.K. (2003) The oxygen fugacity of olivine-phyric martian basalts and the components within the mantle and crust of Mars. *Meteoritics and Planetary Science*, 38, 1793–1805.
- Herd, C.K., Papike, J.J., and Brearley, A.J. (2001) Oxygen fugacity of martian basalts from electron microprobe oxygen and TEM-EELS analyses of Fe-Ti oxides. *American Mineralogist*, 86, 1015–1024.
- Hess, P.C. (1989) *Origins of Igneous Rocks*, 336 p. Harvard University Press, Cambridge, Massachusetts.
- Jones, J.H. (2004) Redox conditions among the terrestrial planets (abstract). Lunar and Planetary Science Conference XXXV no. 1264. Lunar and Planetary Institute, Houston (CD-ROM).
- Karner, J.M., Papike, J.J., and Shearer, C.K. (2003) Olivine from planetary basalts: chemical signatures that indicate planetary parentage and those that record igneous settings and process. *American Mineralogist*, 88, 806–816.
- — — (2004) Plagioclase from planetary basalts: chemical signatures that reflect planetary volatile budgets, oxygen fugacity, and styles of igneous differentiation. *American Mineralogist*, 89, 1101–1109.
- Karner, J.M., Sutton, S.R., Papike, J.J., Shearer, C.K., Jones, J.H., and Newville, M. (2006) Application of a new vanadium valence oxybarometer to basaltic glasses from the Earth, Moon, and Mars. *American Mineralogist*, 91, 270–277.
- Mason, B. and Allen, R.O. (1973) Minor and trace elements in augite, hornblende and pyrope megacrysts from Kakanui, New Zealand. *Journal of Geology and Geophysics*, 16, 935–947.
- McCanta, M.C., Rutherford, M.J., and Jones, J.H. (2004) An experimental study of rare earth partitioning between a shergottites melt and pigeonite: implications for the oxygen fugacity of the martian interior. *Geochimica et Cosmochimica Acta*, 68, 1943–1952.
- McSween, H.Y. and Treiman, A.H. (1998) Martian meteorites. In J.J. Papike, Ed., *Planetary Materials*, 36, p. 6-01–6-50. Reviews in Mineralogy, Mineralogical Society of America, Chantilly, Virginia.
- Meyer, C. (2003) Mars Meteorite Compendium-1998. JSC no. 27672, Revision B, NASA Johnson Space Center, Houston. (Updated at <http://www-curator.jsc.nasa.gov/curator/antmet/mmc/mmc.htm>.)
- Papike, J.J. (1980) Pyroxene mineralogy of the Moon and meteorites. In C.T. Prewitt, Ed., *Pyroxenes*, 7, p. 495–525. Reviews in Mineralogy, Mineralogical Society of America, Chantilly, Virginia.
- — — (1981) Silicate mineralogy of planetary basalts. In R.B. Merrill and R. Ridings, Eds., *Basaltic Volcanism on the Terrestrial Planets*, p. 340–363. Pergamon, New York.
- — — (1998) Comparative planetary mineralogy: chemistry of melt-derived pyroxene, feldspar, and olivine. In J.J. Papike, Ed., *Planetary Materials*, 36, p. 7-01–7-10. Reviews in Mineralogy, Mineralogical Society of America, Chantilly, Virginia.
- Papike, J.J. and Bence, A.E. (1978) Lunar mare versus terrestrial mid-ocean ridge basalts: planetary constraints on basaltic volcanism. *Geophysical Research Letters*, 5, 803–806.
- Papike, J.J. and White, C. (1979) Pyroxenes from planetary basalts: characterization of “other” than quadrilateral components. *Geophysical Research Letters*, 6, 913–916.
- Papike, J.J., Hodges, F.N., Bence, A.E., Cameron, M., and Rhodes, J.M. (1976) Mare basalts: crystal chemistry, mineralogy, and petrology. *Reviews of Geophysics and Space Physics*, 14, 475–540.
- Papike, J.J., Karner, J.M., and Shearer, C.K. (2003) Determination of planetary basalt parentage: a simple technique using the electron microprobe. *American Mineralogist*, 88, 469–472.
- — — (2004) Comparative planetary mineralogy: V/(Cr + Al) systematics in chromite as an indicator of relative oxygen fugacity. *American Mineralogist*, 89, 1557–1560.
- — — (2005) Comparative planetary mineralogy: Valence state partitioning of Cr, Fe, Ti, and V among crystallographic sites in olivine, pyroxene, and spinel from planetary basalts. *American Mineralogist*, 90, 277–290.
- Pun, A. and Papike, J.J. (1996) Unequilibrated eucrites and the equilibrated Juvinas eucrite: pyroxene REE systematics and major-, minor-, and trace-element zoning. *American Mineralogist*, 81, 1438–1451.
- Righter, K., Sutton, S.R., and Newville, M. (2004) Micro-XANES measurements on experimental spinels and the oxidation state of vanadium in spinel-melt pairs. (abstract). Oxygen in the Terrestrial Planets workshop, no. 3010. Lunar and Planetary Institute, Houston (CD-ROM).
- Sato, M., Hickling, N.L., and McLane, J.E. (1973) Oxygen fugacity values of Apollo 12, 14, and 15 lunar samples and reduced state of lunar magmas. Proceedings of the 4<sup>th</sup> Lunar Science Conference, 1061–1079.
- Schweitzer, E.L., Papike, J.J., and Bence, A.E. (1979) Statistical analysis of clinopyroxene from deep-sea basalts. *American Mineralogist*, 64, 501–513.
- Shearer, C.K., McKay, G., Papike, J.J., and Karner, J.M. (2006). Valence state partitioning of vanadium between olivine-liquid in olivine-phyric martian basalts: A clearer window into the martian mantle. *American Mineralogist*, 91, 1565–1573.
- Shirai, N. and Ebihara, M. (2004) Chemical characteristics of a martian meteorite, Yamato 980459. *Antarctic Meteorite Research*, 17, 55–67.
- Stolper, E.M. (1977) Experimental petrology of eucritic meteorites. *Geochimica et Cosmochimica Acta*, 41, 587–611.
- — — (1979) Trace elements in shergottite meteorites: implications for the origins of planets. *Earth and Planetary Science Letters*, 42, 239–242.
- Sutton, S.R. and Newville, M. (2005) Vanadium K XANES of synthetic olivine: valence determinations and crystal orientation effects (abstract). Lunar and Planetary Science Conference XXXVI, no. 2133. Lunar and Planetary Institute, Houston (CD-ROM).
- Sutton, S.R., Jones, K.W., Gordon, B., Rivers, M.L., and Smith, J.V. (1993) Reduced chromium in olivine grains from lunar basalt 15555: X-ray Absorption Near Edge Structure (XANES). *Geochimica et Cosmochimica Acta*, 57, 461–468.
- Sutton, S.R., Karner, J.M., Papike, J.J., Delaney, J.S., Shearer, C.K., Newville, M., Eng, P., Rivers, M., and Dyar, M.D. (2005) Vanadium K Edge XANES of synthetic and natural basaltic glasses and application to microscale oxygen barometry. *Geochimica et Cosmochimica Acta*, 69, 2333–2348.
- Takeda, H., Miyamoto, M., and Duke, M.B. (1976) Pasamonte pyroxenes, a eucritic analogue of lunar pyroxenes. *Meteoritics and Planetary Science*, 11, 372–374.
- Taylor, S.R. (1992) *Solar system evolution: a new perspective*, p. 307. Cambridge University Press, New York.
- Taylor, S.R., Arculus, R., Perfit, M.R., and Johnson, R.W. (1981) Island-arc basalts. In R.B. Merrill and R. Ridings, Eds., *Basaltic Volcanism on the Terrestrial Planets*, p. 193–213. Pergamon, New York.
- Wadhwa, M. (2001) Redox state of Mars’ upper mantle and crust from Eu anomalies in Shergottite pyroxenes. *Science*, 291, 1527–1530.
- Wänke, H., Baddenhausen, H., Blum, K., Cendales, M., Dreibus, G., Hofmeister, H., Kruse, H., Jagoutz, E., Palme, C., Spettel, B., Thacker, R., and Vilcsek, E. (1977) On the chemistry of lunar samples and achondrites. Primary matter in the lunar highlands: a re-evaluation. Proceedings of the Eighth Lunar and Planetary Science Conference, 2191–2213. Lunar and Planetary Institute, Houston.
- Zolensky, M.E., Pieters, C., Clark, B., and Papike, J.J. (2000) Small is beautiful: the analysis of nanogram-sized astromaterials. *Meteoritics and Planetary Science*, 35, 9–29.

MANUSCRIPT RECEIVED SEPTEMBER 26, 2005

MANUSCRIPT ACCEPTED APRIL 17, 2006

MANUSCRIPT HANDLED BY DAVID VANIMAN